J. Fluid Mech. (2006), *vol.* 566, *pp.* 153–162.
doi:10.1017/S0022112006002321 Printed in the United Kingdom

Direct numerical simulation of polymer-induced drag reduction in turbulent boundary layer flow of inhomogeneous polymer solutions

By COSTAS D. DIMITROPOULOS[1,2,3], YVES DUBIEF[1,3], ERIC S. G. SHAQFEH[1,2] AND PARVIZ MOIN[1,3]

[1]Department of Mechanical Engineering, Stanford University, Stanford, CA 94305, USA

[2]Department of Chemical Engineering, Stanford University, Stanford, CA 94305, USA

[3]Center for Turbulence Research, Stanford University, Stanford, CA 94305, USA

(Received 6 March 2006 and in revised form 2 August 2006)

Skin-friction drag reduction in turbulent boundary layer flow of inhomogeneous polymer solutions is investigated using direct numerical simulations. A continuum constitutive model (FENE-P) accounting for the effects of polymer microstructure and concentration is used to describe the effect of viscoelasticity. The evolution of wall friction along the streamwise direction is a function of the dynamics of the polymer distribution in the boundary layer. It is observed that polymer transport decreases drag reduction downstream compared to the homogeneous case. The fluctuations of polymer concentration are anti-correlated with those of the streamwise velocity. Concentration is largest in the low-speed streaks. The physical process creating this effect is primarily that of dilution of the high-speed streaks, where due to the local turbulence structure the dispersion of polymer is strongest. Thus, the polymer-induced drag reduction phenomenon is sustained primarily in the vicinity of the low-speed streaks where the injected polymer additive is most effective.

1. Introduction

Skin-friction drag reduction by polymer additives in turbulent flows has received great attention in the past few years. The renewed interest can be partly attributed to the development of robust methods for direct numerical simulation (DNS) of viscoelastic turbulent flows. Most simulations have been performed in periodic channels where the flow is internal and spatially stationary or for homogeneous turbulence (see for example Dubief *et al.* (2004, 2005) and references therein). Recent work by Dimitropoulos *et al.* (2005) has extended the study to developing external turbulent flows, which are important in naval applications, where zero-pressure-gradient (ZPG) turbulent boundary layer flow is frequently encountered. DNS of drag reduction in homogeneous (constant polymer concentration) viscoelastic ZPG turbulent boundary layers has shown that the development of turbulent structure, including vortex damping, and polymer extension are asynchronous. The spatial evolution is a strong function of polymer elasticity, expressed by the ratio of the relaxation time scale of the molecules to the turbulent wall time scale. For large polymer elasticity drag reduction of up to 60 % can be simulated within a downstream length equal to a few boundary layer thicknesses. A quasi-steady region of drag reduction where the wall friction in both Newtonian and viscoelastic flows evolves with the same rate can also be observed.

All simulations of drag reduction so far have considered homogeneous viscoelastic fluids, but it is of interest to better understand the effect of an inhomogeneous introduction of polymer additives in a turbulent boundary layer. Inhomogeneous turbulent boundary layers have been studied so far only through the use of simple analytical models (Larson 2003). In addition, uncoupled studies of the effect of drag reduction on the transport of a passive scalar have been performed recently (Gupta, Sureshkumar & Khomami 2005). Simulation of flow of inhomogeneous polymer solutions using full coupling between concentration and polymer stress in the momentum equation has received little attention, due to the complexity of the model equations for systems that are not dilute (Beris & Edwards 1994). For dilute systems, work has been restricted to stability analysis of laminar viscometric flows, such as Taylor–Couette flow (Apostolakis, Mavrantzas & Beris 2002). The present investigation constitutes the first DNS of turbulent flow of inhomogeneous polymer solutions. It is performed for a turbulent boundary layer and is designed to resemble polymer injection experiments (White, Somandepalli & Mungal 2004) aiming to understand how to optimize practical drag-reduction strategies.

2. Mathematical formulation

2.1. *Model equations*

Transport phenomena in inhomogeneous, dilute, isothermal and incompressible polymer solutions can be described by a set of model equations derived from the principles of continuum mechanics and non-equilibrium thermodynamics by using a two-fluid Hamiltonian model. By considering a Warner spring force law and utilizing the Peterlin approximation one can arrive at an extended FENE-P model that incorporates concentration effects in a simplified manner (Beris & Edwards 1994; Apostolakis *et al.* 2002).

Specifically, the momentum conservation and continuity equations have the form

$$\frac{\partial u_i}{\partial t} + u_j \frac{\partial u_i}{\partial x_j} = -\frac{\partial p}{\partial x_i} + \frac{\beta}{Re_\theta} \frac{\partial^2 u_i}{\partial x_j^2} - \frac{1-\beta}{Re_\theta} \frac{1}{We} \frac{\partial \tau_{ij}}{\partial x_j}, \tag{2.1}$$

$$\frac{\partial u_i}{\partial x_i} = 0, \tag{2.2}$$

where u_i represents the fluid velocity, p the pressure, x_i the spatial coordinate, t the time and τ_{ij} the viscoelastic extra-stress tensor. The Reynolds number Re_θ is defined with the zero-shear kinematic viscosity of the solution (ν_0) and β is the ratio of zero-shear-rate solvent (μ_s) to solution viscosity (μ_0). The velocity scale is the average value of the streamwise velocity at the free stream, U_{fs}, and the length scale is the momentum thickness, θ, at the inflow location (θ_{in}). We denotes the Weissenberg number, which is equal to the product of the characteristic relaxation time of the polymer (λ) and a characteristic flow shear rate (U_{fs}/θ_{in}).

The distribution of polymer in the flowing solution is described by the following conservation equation:

$$\frac{\partial n}{\partial t} + u_i \frac{\partial n}{\partial x_i} = -\frac{\partial J_i}{\partial x_i}, \tag{2.3}$$

where n is the polymer concentration, expressed as a number density non-dimensionalized with its value at the wall of the inflow plane. Note that the zero-shear solution viscosity in β corresponds to $n = 1$.

The polymer flux J_i includes both Fickian and stress-diffusion terms and is defined as:

$$J_i = -\frac{1}{Pe}\left(\frac{\partial n}{\partial x_i} - \frac{\partial \tau_{ij}}{\partial x_j}\right). \tag{2.4}$$

Pe is the Péclet number, defined as $Pe = U_{fs}\theta_{in}/D$, where D is the translational diffusivity of the polymer molecules in the solvent. The Schmidt number, Sc, expresses the ratio of the zero-shear solution viscosity and the translational diffusivity of the polymer so that $Pe = ScRe_\theta$. Aqueous solutions of polymers used for drag-reduction studies have Schmidt numbers that are $O(10^5)$ (Beris & Edwards 1994; Apostolakis *et al.* 2002). As a result, polymer transport is dominated by advection and in order to improve numerical stability the stress-diffusion term is neglected, since it has a secondary contribution for the flow conditions considered in this study. The Fickian term is retained and is used in conjunction with the dynamic model for large-eddy simulation (LES) (Pierce & Moin 2004) for providing an eddy diffusivity that describes the small-scale transport behaviour at large Sc which cannot be resolved by the computational mesh.

The viscoelastic contribution to the stress is a function of the fluid microstructure and the local polymer concentration. For the FENE-P dumbbell model (Beris & Edwards 1994) it has the form

$$\tau_{ij} = n\left(\frac{1}{1 - c_{kk}/L^2}c_{ij} - \delta_{ij}\right), \tag{2.5}$$

where c_{ij} is the single-molecule conformation tensor, defined as the ensemble-averaged dyad of the end-to-end distance of the polymer chain. The nonlinear entropic spring force law corresponds to the pre-averaged Warner spring function, where L is the maximum admissible polymer chain extension. Finally, δ_{ij} denotes the Kronecker delta.

The conformation tensor is coupled to the fluid velocity through an evolution equation:

$$\frac{\partial c_{ij}}{\partial t} + \hat{u}_k\frac{\partial c_{ij}}{\partial x_k} - c_{ik}\frac{\partial \hat{u}_j}{\partial x_k} - c_{kj}\frac{\partial \hat{u}_i}{\partial x_k} = -\frac{1}{We}\tau_{ij}, \tag{2.6}$$

where the right-hand side is a relaxation term and the left-hand side corresponds to the upper-convected derivative, which ensures material reference frame objectivity. In the context of the two-fluid Hamiltonian model (Apostolakis *et al.* 2002) the upper-convected derivative is based on the polymer phase velocity, $\hat{u}$, defined as the sum of the solvent velocity and the differential velocity of the two components, which is a function of the polymer flux:

$$\hat{u}_k = u_k + J_k/n. \tag{2.7}$$

2.2. *Numerical implementation*

The mathematical model eqations are solved using an extension of the method described in Dimitropoulos *et al.* (2005). The spatial discretization is a second-order finite-volume scheme on a staggered grid, where the velocity variables are placed on the cell edges, whereas the pressure, polymer number density and the conformation tensor are located on the cell centres. High-order compact differencing schemes are used for the divergence of the stress tensor entering the momentum equation and the advection term in the evolution equation for the conformation tensor (Min, Yoo & Choi 2001; Dubief *et al.* 2005). Local artificial dissipation (LAD) is used in the evolution equation for the conformation tensor at all locations where c_{ij} loses

positive-definiteness. In this work the coefficient of the LAD term, κ, is equal to 1 and for CFL ≈ 0.15 affects less than 5% of the nodes. A second-order iterative semi-implicit fractional step method, where the conformation tensor and concentration are staggered in time with respect to the velocity and pressure is used to integrate the equations in time, and a multigrid solver is used for the Poisson equation for the pressure at each iteration (Pierce & Moin 2004).

The dynamic model for subgrid-scale variance and dissipation rate of a conserved scalar is implemented identically to Pierce & Moin (2004). The dynamic model provides closure for the smallest scales due to the large Sc, since the smallest scale for the conserved scalar varies as $\eta_K Sc^{-1/2}$, where η_K is the Kolmogorov scale (Batchelor 1959; Dubief *et al.* 2005). The concentration equation is integrated in time using the second-order QUICK scheme as in Pierce & Moin (2004). The QUICK scheme introduces a third-order dissipative error and can predict scalar values beyond their bound limits, without affecting stability and accuracy. In a typical simulation overshoots are encountered in 0.02 % and undershoots in 2 % of the nodes. Note that values beyond the bounds are not used for computing the polymer stress, and the bound limits are used instead. For the correction in the polymer phase velocity, the logarithm of n is used to avoid singularities, along with a tolerance of 10^{-15} for very small values of n to ensure zero flux correction in regions without polymer, typically well-outside the concentration boundary layer.

The inflow boundary condition for the velocity is supplied from a Newtonian simulation which uses an inflow profile constructed by recycling from a downstream station. At the free stream (fs) a combination of Neumann and Dirichlet conditions describing the growth of the boundary layer were used:

$$\frac{\partial u}{\partial y} = 0\bigg|_{fs}, \qquad \frac{\partial w}{\partial y} = 0\bigg|_{fs}, \qquad v_{fs} = U_{fs}\frac{\partial \delta^*(x)}{\partial x}, \tag{2.8}$$

where u, v, w are streamwise, wall-normal and spanwise velocity components, U_{fs} is the reference streamwise free-stream velocity, x, y are the streamwise and wall-normal co-ordinates and $\delta^*(x)$ is the displacement thickness. A convective boundary condition is used at the outflow plane and no-slip is applied on the wall. For the conformation tensor, one-sided conservative compact difference schemes are used to compute derivatives in the streamwise and wall-normal boundaries. In addition, the polymer is introduced under equilibrium conformation (polymer molecules under no initial stress; not pre-stretched) at the inflow plane. The concentration inlet boundary condition corresponds to a constant Gaussian profile that varies only in the wall-normal direction:

$$n_{inflow} = \mathrm{e}^{-(y-a)^2/b} \tag{2.9}$$

At the outflow and free-stream planes convective boundary conditions are applied in order to remove the scalar from the computational domain (Pierce & Moin 2004). Periodic conditions are applied to all variables in the spanwise direction, z.

3. Simulation conditions

We will focus on DNS of two cases of viscoelastic turbulent boundary layer flow, comparing the inhomogeneous with the homogeneous case. The rheological parameters correspond to the high drag reduction regime (HDR) when used for simulations with the homogeneous FENE-P model (Dimitropoulos *et al.* 2005). The maximum extensibility, L, of the FENE-P spring is set to 100 and the solvent viscosity ratio,

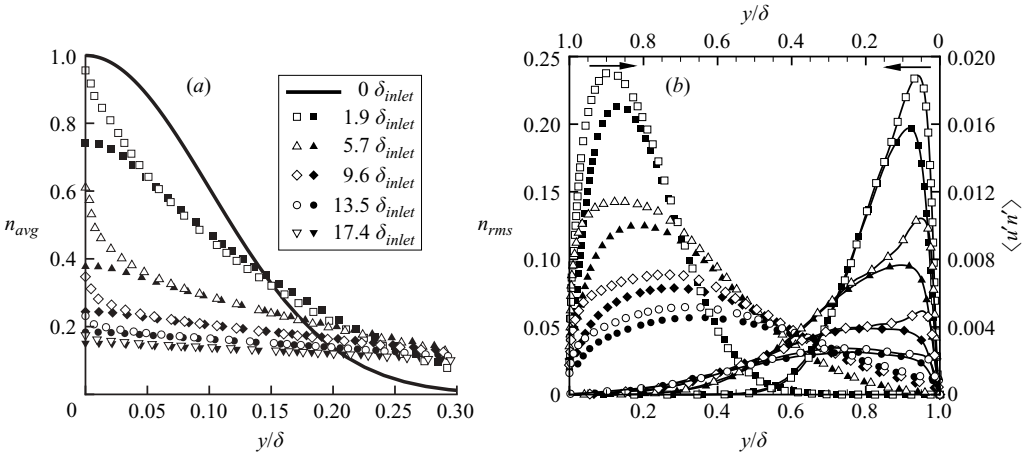

FIGURE 1. Resolvable passive scalar concentration field at different streamwise locations: (*a*) mean, (*b*) root-mean-square fluctuations and streamwise advective mass flux. Filled symbols: $Sc = 1$. Open symbols: $Sc = 1000$.

β, is equal to 0.9. The Weissenberg number (based on the Newtonian wall shear rate at the inflow plane), We_τ, is equal to 50. The molecular Schmidt number considered here is 1000 and stress diffusion can be neglected. The Reynolds number, Re_θ, is approximately 775 at the inflow plane. The Newtonian simulation providing inflow data has $Re_\theta = 670$ at its inlet. The inflow profile (2.9) for the polymer number density corresponds to $a = 0$ and $b = \theta_{in}^2/3$ and is practically zero beyond $y/\delta = 0.3$. The size of the computational domain is $168.4\theta_{in} \times 24.5\theta_{in} \times 32.2\theta_{in}$. The grid size is $480 \times 96 \times 192$ in the streamwise, wall-normal, and spanwise directions, respectively. The domain length is approximately 19 inlet boundary layer thicknesses (δ_{inlet}), where $\delta \equiv \delta_{99.5}$. The corresponding mesh spacing in wall units, which unless otherwise indicated are defined with the inlet friction velocity, is $\Delta x^+ = 13.2$, $\Delta y^+ = (0.11{-}30.6)$ (a hyperbolic tangent stretching function is used) and $\Delta z^+ = 6.3$, providing sufficient resolution for the cases considered (Dubief *et al.* 2004). The simulations were carried out for approximately 4400 inertial units, defined with θ_{in}/U_{fs}, which was adequate for reaching a stationary state and collecting statistics during the final two flow-through times of the simulation.

4. Passive scalar dispersion in a Newtonian turbulent boundary layer

Passive scalar dispersion in a Newtonian turbulent boundary layer is quite effective even for lower Re than those considered here. Figures 1(*a*) and 1(*b*) show the mean profiles, the root-mean-square fluctuations of the resolvable scalar concentration and the variation of the streamwise advective mass flux for a DNS performed for $Re_\theta = 775$ on the same computational domain and resolution as the viscoelastic case. For $Sc = 1$ DNS was used, whereas for $Sc = 1000$ LES was used to model the subgrid-scale terms in the scalar equation. Note that the LES model is limited to $Sc = 1000$ since beyond this value it is not possible to resolve the additional small scales of the concentration field with the present mesh. Figure 1(*a*) shows that for $Sc = 1$ the inflow profile of the injected scalar relaxes rapidly within the relatively small streamwise distance studied here, whereas the effect of the larger Sc is that the concentration very close to the wall is larger and its profile sharper. In addition, figure 1(*b*) shows that as the mass diffusivity decreases the fluctuations of the concentration

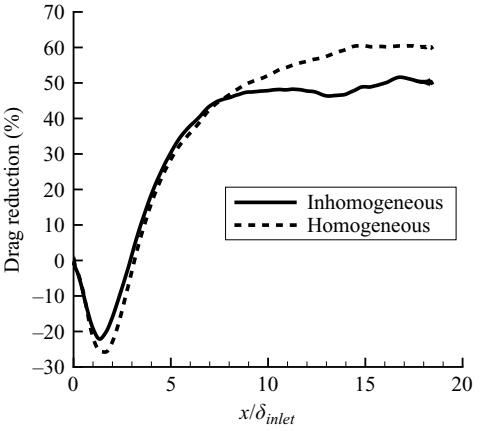

FIGURE 2. Evolution of drag reduction along the length of the boundary layer.

and the streamwise advective mass flux are larger. For large Sc, the concentration fluctuations show first a small shift of their peak to the wall, followed by a rapid decrease to a form similar to that for low Sc. The streamwise advective mass flux follows almost self-similar development like the mean profiles, and is dominated by the near-wall dispersion. Since the largest value of Sc considered in this work is 1000, and for polymers in aqueous solutions $Sc = O(10^5)$ it is not possible to distinguish transport differences due to variation in the mass diffusivity of specific molecules with the present simulation conditions. However, the physical picture described with the present model for the Newtonian case is clearly distinguishable from the viscoelastic case presented below.

5. Comparison of inhomogeneous and homogeneous drag rduction

The predicted drag reduction along the length of the boundary layer is plotted in figure 2. For both inhomogeneous and homogeneous ($n = 1$) cases drag reduction is observed after an initial drag increase where the substantial stretching of polymer after the inlet removes a large amount of energy from the Newtonian flow field, which is redistributed downstream in the flow for drag reduction to occur (Dimitropoulos *et al.* 2005; Dubief *et al.* 2004). As expected, the effects due to the viscoelasticity in the inhomogeneous flow are stronger close to the inflow and are comparable to the homogeneous case. At these locations the polymer concentration remains large enough so that the two terms of the divergence of the viscoelastic extra stress for the inhomogeneous case have a combined contribution comparable in magnitude close to the wall to that of the homogeneous case. As we proceed downstream and the polymer is depleted from the wall, the body forces due to the polymer decrease, leading to a decrease in the observed drag reduction, which is approximately 10 % smaller than the homogeneous case.

The mean streamwise velocity profile after an initial small drag increase shows both the characteristic upward shift of the logarithmic law region compared to the Newtonian case (inflow location) and a change in its slope (figure 3*a*). The main difference compared to the homogeneous simulations (Dimitropoulos *et al.* 2005) is that within the computational domain the slope and intercept change of the logarithmic region are smaller and although the predicted drag reduction is less, the decrease of its magnitude is not due to polymer elasticity as in LDR (low drag reduction). The smaller drag reduction up to a given streamwise position is due

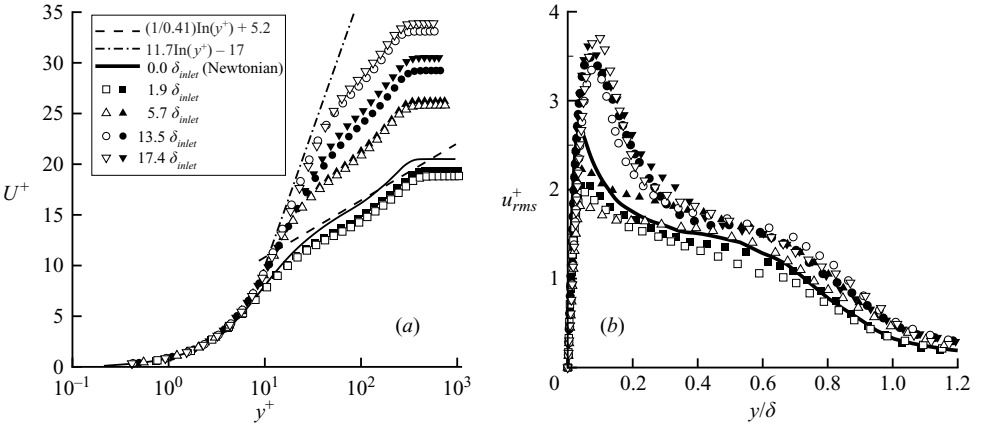

FIGURE 3. (*a*) Average streamwise velocity and (*b*) root-mean-square fluctuations of streamwise velocity along the length of the boundary layer. $(1/0.41)\ln(y^+)+5.2$ is the logarithmic law (dashed line) and $11.7\ln(y^+)-17$ the maximum drag reduction asymptote (dot-dashed line). The statistics are normalized with the local friction velocity. Open symbols: homogeneous case, filled symbols: inhomogeneous case.

to homogenization of the polymer concentration by the turbulence. This is further shown by the streamwise velocity fluctuations (figure 3*b*) that follow similar trends and an increase in their magnitude downstream due to drag reduction decrease is not observed within the computational domain. The development region of drag reduction for inhomogeneous flows is now a function of both elasticity and concentration. As observed in figure 2, drag reduction is smaller and tends to plateau further upstream than in the homogeneous case owing to the decrease of concentration, and persists throughout the remaining computational domain, an indication that although the concentration decreases the polymer deformation remains large enough to sustain vortex damping downstream. The lack of polymer beyond the logarithmic layer ($y/\delta > 0.3$) makes the transition from a viscoelastic to a Newtonian flow field the only factor that can change the qualitative form of the velocity statistics. The small differences between the homogeneous, inhomogeneous and Newtonian simulations in the outer region confirm that the effect of additive transport is confined to the near-wall region.

Figure 4 provides further evidence of the near-wall character of drag reduction and shows the depletion of the polymer. The average concentration profile (figure 4*a*) evolves downstream in a manner different to the case of passive scalar dispersion in a Newtonian turbulent boundary layer (figure 1*a*). It is clear that the character of dispersion is different and the efficiency of the flow in transporting the polymer away from the wall is significantly decreased. The viscoelastic case shows that the concentration profile becomes sharper due to the large *Sc* but also retains larger values close to the wall. This slow decrease is indicative of the decrease of the intensity of the wall-normal velocity fluctuations during drag reduction that contribute most significantly to dispersion. The physical process is that the events generating turbulence are less frequent and the streamwise vortices become weaker and larger, losing some of their ability to promote transport in the wall-normal direction. As a result, the rate of transport of the injected polymer away from the buffer layer is reduced. This in turn corresponds to a lower rate of polymer additive transport beyond the logarithmic layer, where the flow is increasingly Newtonian in character and mixing is more efficient, resulting in decreased polymer depletion in addition to

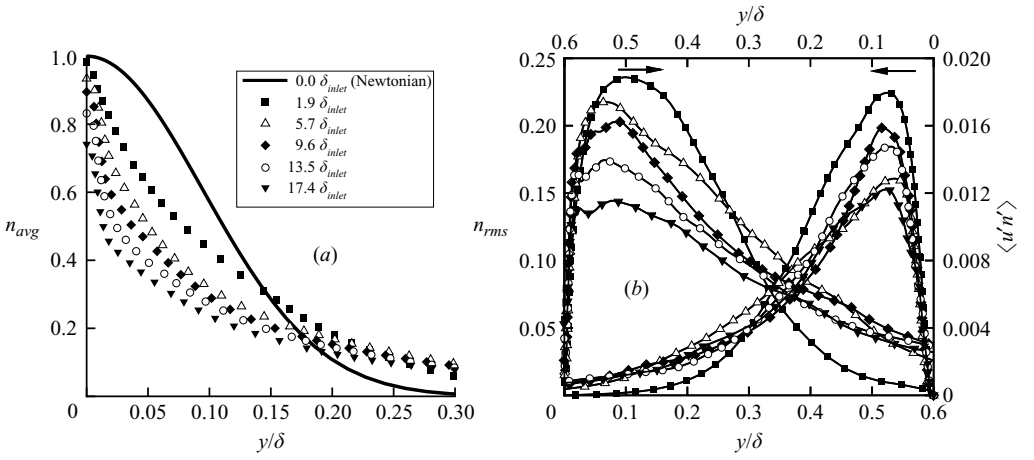

FIGURE 4. Resolvable polymer number density field at different streamwise locations: (*a*) mean, (*b*) root-mean-square fluctuations and streamwise advective mass flux.

slower sharpening of the mean concentration profile. However, for both Newtonian and viscoelastic flow, there is evidence of self-similar development, although the functional form for each case is different. The evolution of the root-mean-square fluctuations of the concentration (figure 4*b*) is consistent with the above physical description. Comparison with the case of passive scalar in a Newtonian boundary layer (figure 1*b*), reveals a significant persistence of the structure of the concentration field for the viscoelastic case, where a slow shift of the profile peak towards the wall and a significant decrease in magnitude for $y/\delta > 0.2$ are observed. The form of these concentration statistics suggests that the layer of polymer retained close to the wall undergoes significant interaction with the near-wall structures even at large distances downstream. The advective streamwise mass flux also plotted in figure 4(*b*) develops in a similar way to drag reduction and the velocity fluctuations. There is an initial decrease followed by a rapid increase and then a slower decrease as the additive is mixed downstream. After the initial development region its magnitude is larger than for Newtonian flow, corresponding to enhanced transport in the streamwise direction, an observation consistent with experiment (Somandepalli 2006) and uncoupled simulations (Gupta *et al.* 2005).

Larson (2003) proposed an analytic model of drag reduction in a turbulent boundary layer, which predicts that maximum drag reduction (MDR) cannot be sustained for a single injection of polymer. However, it does not include treatment of the modified polymer transport in the near-wall region, which is important given experiments (for example White *et al.* 2004) showing that HDR can be sustained for significant distances downstream owing to the reduced transport of polymer away from the wall. The present simulations have similar trends to experiment and provide additional information reinforcing the conclusion that the driving force for polymer transport is primarily affected by the near-wall dynamics and not the outer region.

The increase of the Newtonian character of the flow with distance from the wall is evident from figure 5 where the amount of polymer deformation (the average of the trace of the conformation tensor) is plotted for different streamwise locations. In the inhomogeneous data, there is much larger extension beyond $y/\delta \approx 0.3$, which is a result of the existence of regions with little polymer where drag reduction is small and the flow field being closer to Newtonian. In such locations, where there

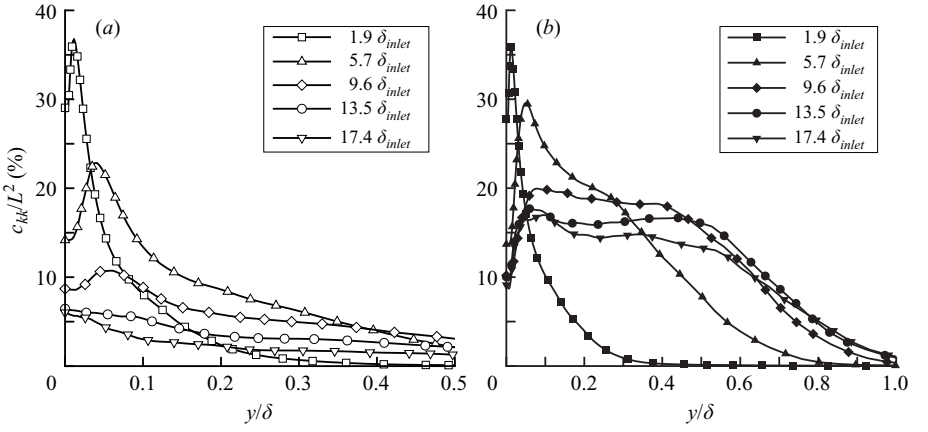

FIGURE 5. Polymer extension (c_{ij}) along the wall-normal coordinate at different streamwise locations: (*a*) homogeneous, (*b*) inhomogeneous.

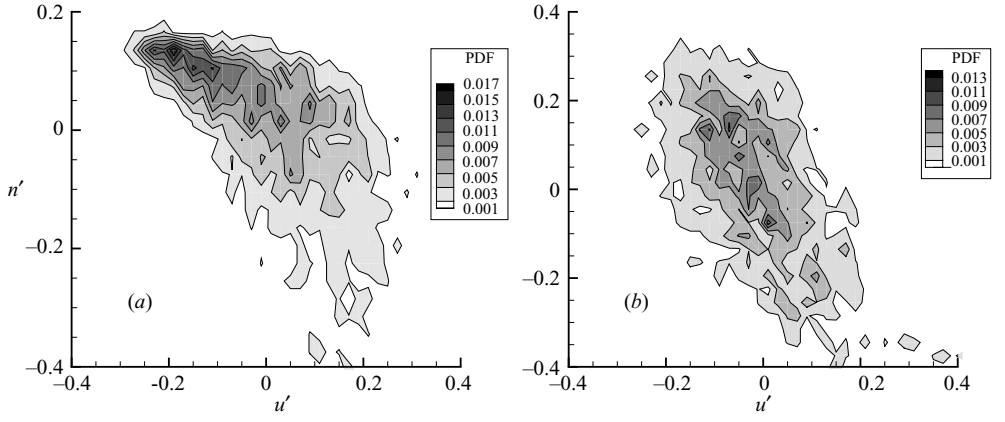

FIGURE 6. Joint probability distribution function for velocity and concentration fluctuations at $y^+ = 15$: (*a*) $x = 1.9\delta_{inlet}$, (*b*) $x = 13.5\delta_{inlet}$.

is less damping of the flow, the relative intensity of the velocity gradient increases resulting in the prediction of larger polymer extension by the evolution equation for the single-molecule conformation tensor. The characteristic peak in the buffer layer, which close to the inflow corresponds to the contribution of the streamwise vortices (Dimitropoulos *et al.* 2005; Dubief *et al.* 2004) tends to move towards the wall downstream as drag reduction increases and the contribution of the mean shear becomes more important. However, in contrast to the homogeneous case the off-wall peak is retained and the maximum extension does not shift to the wall. The form of the statistics of the conformation indicate that they are affected by variations in the spanwise direction, namely the existence of regions near the wall where there are small amounts of polymer present. Experimental evidence (M. G. Mungal 2005, personal communication) shows that the polymer additive resides in the low-speed streaks. This effect is observed in the present simulations. Figure 6 shows the joint probability distribution function (PDF) for the streamwise velocity and concentration fluctuations at two streamwise locations and at a distance from the wall close to the edge of the buffer layer. The (PDF) shows strong anti-correlation of streamwise

velocity and concentration, which persists downstream owing to reduced mixing observed in drag-reduced flow, a strong indication that the polymer resides in the low-speed streaks. Therefore, since the events corresponding to large fluctuations of polymer concentration are dominant in the low-speed streaks, it also follows that most of the effective polymer is located there and thus injection efficiency is not constant across the spanwise direction.

6. Conclusions

A method for direct numerical simulation of inhomogeneous viscoelastic turbulent boundary layer flow has been developed and used to investigate drag reduction after additive injection. It was observed that polymer mixing acts as a relaxation mechanism for drag reduction. The effect of polymer depletion is not rapid, since the modified structure of the turbulent flow field assists in retaining the additive in the near-wall region. The development of drag reduction for inhomogeneous flows, in addition to the elasticity and extensibility of the polymer molecules, depends on the evolution of the near-wall concentration, which exhibits the development of a more persistent thin layer next to the wall, enhanced advective transport in the streamwise direction and additive segregation between the wall-layer streaks. The simulation predictions for the interaction of polymer transport and drag reduction presented in this work are in qualitative agreement with recent experimental observations.

The support of DARPA (Grant No. MDA972-03-1-0033-P00006) is acknowledged. We thank the members of the Stanford FDR Group for insightful discussions.

REFERENCES

Apostolakis, M. V., Mavrantzas, V. G. & Beris, A. N. 2002 Stress gradient-induced migration effects in the taylor-couette flow of a dilute polymer solution. *J. Non-Newtonian Fluid Mech.* **102**, 409–445.

Batchelor, G. K. 1959 Small-scale variation of convected quantities like temperature in turbulent fluid. Part 1. General discussion and the case of small conductivity. *J. Fluid Mech.* **5**, 113–133.

Beris, A. N. & Edwards, B. J. 1994 *Thermodynamics of Flowing Systems with Internal Microstructure*. Oxford University Press.

Dimitropoulos, C. D., Dubief, Y., Shaqfeh, E. S. G., Moin, P. & Lele, S. K. 2005 Direct numerical simulation of polymer-induced drag reduction in turbulent boundary layer flow. *Phys. Fluids* **17**, 011705-1–011705-4.

Dubief, Y., Terrapon, V. E., White, C. M., Shaqfeh, E. S. G., Moin, P. & Lele, S. K. 2005 New answers on the interaction between polymers and vortices in turbulent flows. *Flow, Turbulence Combust.* **74**, 311–329.

Dubief, Y., White, C. M., Terrapon, V. E., Shaqfeh, E. S. G., Moin, P. & Lele, S. K. 2004 On the coherent drag-reducing and turbulence-enhancing behaviour of polymers in wall flows. *J. Fluid Mech.* **514**, 271–280.

Gupta, V. K., Sureshkumar, R. & Khomami, B. 2005 Passive scalar transport in polymer drag reduced turbulent flow. *AIChE J.* **51**, 1938–1950.

Larson, R. G. 2003 Analysis of polymer turbulent drag reduction in flow past a flat plate. *J. Non-Newtonian Fluid Mech.* **111**, 229–250.

Min, T., Yoo, J. & Choi, H. 2001 Effect of spatial discretization schemes on numerical studies of viscoelastic flows. *J. Non-Newtonian Fluid Mech.* **100**, 27–47.

Pierce, C. D. & Moin, P. 2004 Progress-variable approach for large-eddy simulation of non-premixed turbulent combustion. *J. Fluid Mech.* **504**, 73–97.

Somandepalli, V. S. R. 2006 Combined PIV and PLIF measurements in a polymer drag reduced turbulent boundary layer. PhD thesis, Stanford University.

White, C. M., Somandepalli, V. S. R. & Mungal, M. G. 2004 The turbulence structure of drag reduced boundary layer flow. *Exps. Fluids* **36**, 62–69.